

Biased Backpressure Routing Using Link Features and Graph Neural Networks

Zhongyuan Zhao, *Member, IEEE*, Bojan Radojičić, Gunjan Verma, Ananthram Swami, *Life Fellow, IEEE*, and Santiago Segarra, *Senior Member, IEEE*

Abstract—To reduce the latency of Backpressure (BP) routing in wireless multi-hop networks, we propose to enhance the existing shortest path-biased BP (SP-BP) and sojourn time-based backlog metrics, since they introduce no additional time step-wise signaling overhead to the basic BP. Rather than relying on hop-distance, we introduce a new edge-weighted shortest path bias built on the scheduling duty cycle of wireless links, which can be predicted by a graph convolutional neural network based on the topology and traffic of wireless networks. Additionally, we tackle three long-standing challenges associated with SP-BP: optimal bias scaling, efficient bias maintenance, and integration of delay awareness. Our proposed solutions inherit the throughput optimality of the basic BP, as well as its practical advantages of low complexity and fully distributed implementation. Our approaches rely on common link features and introduces only a one-time constant overhead to previous SP-BP schemes, or a one-time overhead linear in the network size to the basic BP. Numerical experiments show that our solutions can effectively address the major drawbacks of slow startup, random walk, and the last packet problem in basic BP, improving the end-to-end delay of existing low-overhead BP algorithms under various settings of network traffic, interference, and mobility.

Index Terms—Backpressure, MaxWeight scheduling, shortest path, queueing networks, last packet problem, graph neural networks.

I. INTRODUCTION

Backpressure (BP) routing [3] is a well-established algorithm for distributed routing and scheduling in wireless multi-hop networks. Wireless multi-hop networks have been widely adopted in military communications, disaster relief, and wireless sensor networks, and are envisioned to support emerging applications such as connected vehicles, robotic swarms, Internet of Things, machine-to-machine communications, and 5G/6G (device-to-device, wireless backhaul, integrated access and backhaul, and non-terrestrial coverage) [4]–[11]. The distributed nature of BP algorithms [1]–[3], [12]–

Z. Zhao and S. Segarra are with the Department of Electrical and Computer Engineering, Rice University, USA. e-mails: {zhongyuan.zhao, segarra}@rice.edu

B. Radojičić is with the Faculty of Technical Sciences, University of Novi Sad, Serbia. e-mail: bojanradojicic00@gmail.com. Work was done as a visiting scholar at Rice University.

G. Verma, and A. Swami are with the US Army's DEVCOM Army Research Laboratory (ARL), USA. e-mails: {gunjan.verma.civ, ananthram.swami.civ}@army.mil.

Research was sponsored by the DEVCOM ARL Army Research Office and was accomplished under Cooperative Agreement Number W911NF-19-2-0269. The views and conclusions contained in this document are those of the authors and should not be interpreted as representing the official policies, either expressed or implied, of the Army Research Office or the U.S. Government. The U.S. Government is authorized to reproduce and distribute reprints for Government purposes notwithstanding any copyright notation herein.

Preliminary results were presented in [1], [2].

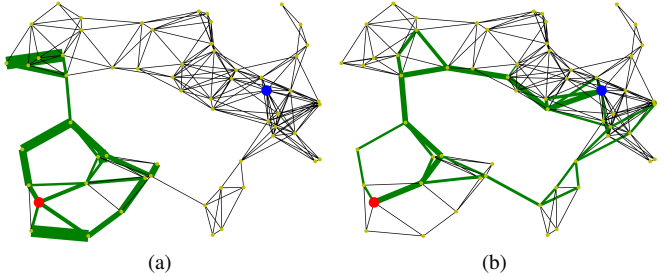


Fig. 1: A flow from the red node to the blue node in a wireless multi-hop network with 60 nodes. The width of an edge is $1 + \sqrt[3]{n}$, where n is the number of packets sent over that link in 500 time steps; green edges indicate routes ($n > 0$). (a) Basic BP routing. (b) Enhanced dynamic BP routing (EDR) [12], [13] with a pre-defined bias given by a scaled shortest hop distance from a node to the destination.

[26] enables wireless multi-hop networks to be self-organized without relying on infrastructure, and promotes scalability and robustness that are critical to many applications. BP has also been adopted to maximize the throughput of TCP networks [27]. In BP, each node maintains a separate queue for packets to each destination (also denominated as commodity), routing decisions are made by selecting the commodity that maximizes the differential backlog between the two ends of each link, and data transmissions are activated on a set of non-interfering links via MaxWeight scheduling [3], [28], [29]. This mechanism uses congestion gradients to drive data packets towards their destinations through all possible routes, avoiding congestion and stabilizing the queues in the network for any flow rate within the network capacity region – a property known as *throughput optimality* [3], [12]–[14].

However, classical BP routing is known to suffer from poor delay performance, especially under low-to-medium traffic loads [12]–[17], exhibiting three drawbacks: 1) *slow startup*: when a flow starts, many packets have to be first backlogged to form stable queue backlog-based gradients, causing large initial end-to-end delay; 2) *random walk*: during BP scheduling, the fluctuations in queue backlogs drive packets toward random directions, causing unnecessarily long routes or loops; and 3) the *last packet problem* [18], [19]: packets of a short-lived flow could remain enqueued in the network for a long time due to the absence of pressure. The phenomena of slow startup and random walk in basic BP routing are illustrated by the example in Fig. 1(a), in which packets from the red source node did not reach their blue destination in the first 500 time slots, but were trapped in two loops shown by the thickest green edges.

There are two categories of low-overhead BP variations for latency improvement: 1) Biased BP adds pre-defined queue-agnostic biases, e.g., (functions of) shortest path distance [1], [2], [12], [13], [15] to the backlog metric. Shortest path-biased BP (SP-BP) can mitigate the drawbacks of slow startup and random walk, while maintaining throughput optimality [12], [13], [15] at a low cost, i.e., a one-time communication overhead for bias computation. As exemplified in Fig. 1(b), two major routes around the empty central area can be quickly established by SP-BP [12], [13]. 2) Delay-based BP employ delay-based backlog metrics rather than queue length [16], [19], [21], in order to address the last packet problem and to stabilize the queues in the network. Importantly, the aforementioned approaches do not require additional communication overhead at every time step, unlike those based on queue state information (QSI) of the network [16], [17] or virtual queues [18], [20] (see Section II-A for a more detailed survey). However, to get the most out of these approaches, careful parameter tuning is required, typically done via trial-and-error.

In this work, we aim to improve the SP-BP routing [1], [12], [13] in the presence of short-lived traffic and network mobility, while retaining its low computational and communication overhead and throughput optimality. Specifically, we seek to improve the widely-used shortest hop-distance bias [12], [13], [15], [23], [24] by considering differences in the scheduling duty cycle of wireless links rather than treating all links equally. This can improve routing decisions by avoiding hot-spots with many interfering neighbors (i.e., high betweenness centrality [30]). However, link duty cycles are deeply intertwined with routing and scheduling schemes, thus cannot be directly observed by passive monitoring. As a result, we propose to predict them with a graph neural network (GNN) [31] informed by the interference topology and traffic statistics.

Furthermore, we also address three longstanding challenges associated with SP-BP [2]: 1) how to optimize the scaling of the shortest path bias or edge weights; 2) how to efficiently update the shortest path bias under node mobility, e.g., nodes moving, joining or leaving the network; and 3) how to effectively incorporate delay-based backlog metrics into SP-BP in response to the last packet problem.

Contribution. The contributions of this paper are as follows:

- We enable the application of GNNs to enhance SP-BP by proposing a model-based framework and a customized offline reinforcement learning (RL) scheme. The GNN incorporates delay awareness into the shortest path biases by predicting link scheduling duty cycles.
- We develop principled approaches for optimal scaling and efficient maintenance of the shortest path biases. Optimal bias scaling mitigates random walk behavior and the last packet problem, while efficient bias maintenance makes SP-BP adaptive to network mobility with low overhead.
- We propose $\exp Q$ [2], a new delay-based backlog metric that prioritizes older packets without tracking packet sojourn time. The $\exp Q$ can be seamlessly integrated into SP-BP, and we further prove its throughput optimality.
- We numerically evaluate our enhancements to SP-BP, demonstrating their effectiveness in improving the latency

and packet delivery rate under varying information availability, as well as their impact on network capacity.

Notation: The following notational convention is adopted in this paper: $(\cdot)^\top$, \odot , and $|\cdot|$ represent the transpose operator, Hadamard (element-wise) product operator, and the cardinality of a set, respectively. $\mathbb{1}(\cdot)$ is the indicator function. $\mathbb{E}(\cdot)$ stands for expectation. Upright bold lower-case symbol, e.g., \mathbf{z} , denotes a column vector, and \mathbf{z}_i denotes the i -th element of vector \mathbf{z} . Upright bold upper-case symbol \mathbf{Z} denotes a matrix, of which the element at row i and column j is denoted by \mathbf{Z}_{ij} , the entire row i by \mathbf{Z}_{i*} , and the entire column j by \mathbf{Z}_{*j} .

II. RELATED WORK

A. Backpressure Routing

Backpressure (BP) routing and scheduling was first proposed in [3]. Four categories of BP variations have been developed to improve the latency of basic BP: 1) Biased BP adds pre-defined queue-agnostic biases, e.g., (functions of) shortest path distance [1], [2], [12], [13], [15] to the backlog metric. SP-BP can mitigate the drawbacks of slow startup and random walk, while maintaining throughput optimality [12], [13], [15] at a low cost, i.e., a one-time communication overhead for bias computation. 2) Delay-based BP replaces queue-length with delay metrics [16], [19], [21] for the backlog. This approach addresses the last packet problem and maintains throughput optimality. 3) Impose restrictions on the routes [22], [23] or hop counts [24] to prevent or reduce loops. However, schemes in 2) and 3) can often shrink the network capacity region. 4) Use queue-dependent biases that aggregate the queue state information (QSI) of the local neighborhood (or global QSI) to improve myopic BP decisions [16], [17] or use shadow queues [18], [20] to dynamically increase the backpressure. This, however, requires nodes to collect the neighborhood or global QSI at each time step, leading to high communications costs. In addition, most of the aforementioned approaches require careful parameter tuning, typically done via trial-and-error. Our work seeks to enhance low-overhead SP-BP by incorporating link and topological information, integrating delay-based backlog metrics, and establishing principles for optimal parametric setting.

BP routing has also been extended to broader applications, such as wireless networks with intermittent connections [18], [26] or uncertain network states [25]. More broadly, BP routing has been modified to maximize the throughput of TCP networks [27] by replacing the backlog-based backpressure with other traffic statistics. Another related area is Universal Max Weight [32], which extends the BP schemes from uni-cast to anycast, multi-cast, and broadcast, and has been adopted in wireless software-defined networks (SDN) [33].

B. GNNs for Wireless Resource Allocation

GNNs are powerful machine learning (ML) tools that can exploit the communications network structure while maintaining permutation equivariance, a key inductive bias for graph-based tasks, stating that the indexing of nodes in a graph shall not affect their representation [31]. As a result, GNNs have been recently applied for various resource allocation problems

in wireless networks, including power allocation [34]–[41] and link scheduling [29], [42]–[45]. For routing, GNNs have been applied to enhance distributed combinatorial solvers for multicast routing, cluster head election, and virtual backbone establishment in wireless multihop networks [46], model-free routing algorithm in wired networks [47], and to develop digital twins to efficiently predict the performance of routing schemes, replacing computationally costly network simulators [48], [49]. GNNs have also been applied to inform decisions in computational offloading by processing the subtask dependency relationship and network context [50], [51]. To the best of our knowledge, this is the first work to apply GNNs to enhance BP routing and scheduling.

While supervised learning has been utilized to train GNNs in some tasks like the digital twin [48], [49] for routing performance prediction, generally speaking, generating high-quality training labels can be computationally intractable since many resource allocation tasks are NP-hard [45]. To address this challenge, schemes of unsupervised learning [34]–[37], primal-dual learning [38]–[41], and reinforcement learning (RL) [29], [42]–[44], [46], [47] have been developed. Following the methodology in [29], [42]–[44], [46] of using GNNs to augment a conventional discrete algorithmic framework, we enhance the biased SP-BP scheme by link duty cycle predicted by GNNs. Moreover, our usage of the conflict graph in predicting link duty cycles is inspired by its use in link scheduling in [29], [42]–[44]. Our customized RL scheme enables GNNs to learn by interacting with the networking environment. Even though our loss function is the mean-square-error between the predicted and empirical link duty cycles, our training approach differs from supervised learning since the predicted link duty cycles will affect routing and scheduling decisions, and subsequently, the empirical link duty cycles. However, unlike the RL schemes in [29], [42]–[44], [46], our loss function is decoupled from the system objective, i.e., the average end-to-end delay of data packets. Thus, our RL scheme circumvents the credit assignment challenge in attributing the contribution of individual link duty cycles to the average end-to-end delay over a chain of SP-BP steps.

III. SYSTEM MODEL AND BACKPRESSURE ALGORITHM

To understand the system model and the basic SP-BP algorithm, the readers can refer to the overall architecture of our proposed SP-BP scheme as illustrated in Fig. 2.

A. System Model

We model a wireless multi-hop network as an undirected graph $\mathcal{G}^n = (\mathcal{V}, \mathcal{E})$, where \mathcal{V} is a set of nodes representing user devices in the network, and \mathcal{E} represents a set of links, where $e = (i, j) \in \mathcal{E}$ for $i, j \in \mathcal{V}$ represents that node i and node j can directly communicate. \mathcal{G}^n is called a connectivity graph and assumed to be a connected graph, i.e., two arbitrary nodes in the network can always reach each other. Notice that routing involves directed links, so we use (i, j) to denote data packets being transmitted from node i to node j over link (i, j) . There is a set of flows \mathcal{F} in the network, in which a flow $f = (i, c) \in \mathcal{F}$, where $i \neq c$ and $i, c \in \mathcal{V}$, describes the stream of packets

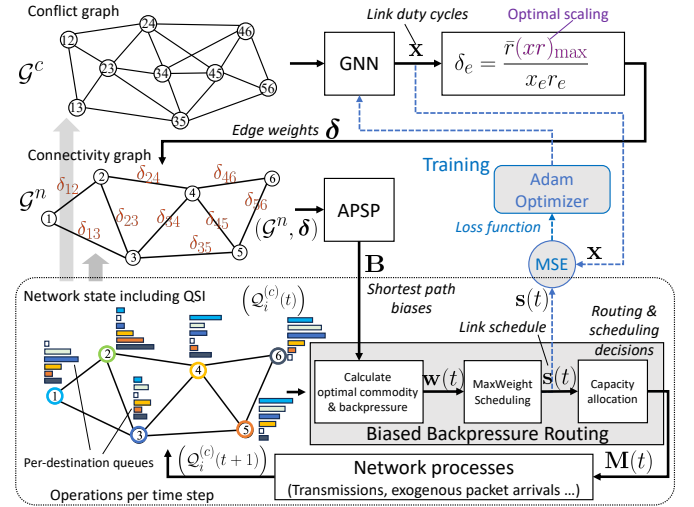


Fig. 2: System diagram of our GNN-enhanced SP-BP scheme.

from a source node i to a destination node (or commodity) c , potentially through multiple links. The medium access control (MAC) of the wireless network is assumed to be time-slotted orthogonal multiple access. Each time slot t contains a stage of decision-making for routing and scheduling, followed by a second stage of data transmission. Each node hosts multiple queues, one for each flow destined to commodity $c \in \mathcal{V}$. We use $Q_i^{(c)}(t)$ to denote the QSI of commodity c at node i at the beginning of time slot t , and $Q_i^{(c)}(t)$ for its queue length. Like earlier works on BP [3], [12]–[26], we assume an infinite queue buffer length to study the impact of the proposed SP-BP on network congestion.

Matrix $\mathbf{R} \in \mathbb{Z}_+^{|\mathcal{E}| \times T}$ collects the (stochastic) real-time link rates, of which an element $\mathbf{R}_{e,t}$ represents the number of packets that can be delivered over link e in time slot t . The long term link rate of a link $e \in \mathcal{E}$ is denoted by $r_e = \mathbb{E}_{t \leq T} [\mathbf{R}_{e,t}]$, vector of long term link rates $\mathbf{r} = [r_e | e \in \mathcal{E}]$, and $\bar{r} = \mathbb{E}_{e \in \mathcal{E}, t \leq T} [\mathbf{R}_{e,t}]$ is the network-wide average link rate.

To describe the conflict relationships between wireless links under orthogonal multiple access, we define *conflict graph*, $\mathcal{G}^c = (\mathcal{E}, \mathcal{C})$, as follows: a vertex $e \in \mathcal{E}$ represents a link in the original network, and the presence of an undirected edge $(e_1, e_2) \in \mathcal{C}$ means that simultaneous communications on links $e_1, e_2 \in \mathcal{E}$ cause interference. There are two popular models for the conflict relationship between two links: 1) Interface conflict, which describes that two links sharing the same node cannot be turned on simultaneously when each node is equipped with only one radio transceiver. The interface conflict model captures scenarios in which all mobile devices are equipped with antennas with beamforming capabilities, such as mmWave/THz massive MIMO. The conflict graph under interface conflict model is given by the line graph of the connectivity graph. 2) Physical distance interference model [52], which arises when two links interfere with each other if their incident nodes are within a certain distance such that their simultaneous transmission will cause the outage probability to exceed a prescribed level. We consider the unit-disk interference model that captures a simplified scenario in

which all the mobile devices transmit at identical power levels with an omnidirectional antenna, and two links conflict with each other if they share the same node or if any of their nodes are within a pre-defined distance. For the rest of this paper, we assume the conflict graph \mathcal{G}^c to be known, e.g., by each link monitoring the wireless channel [44]. See the lower left of Fig. 2 for the QSI, connectivity graph \mathcal{G}^n , and conflict graph \mathcal{G}^c of a small exemplary network.

B. Backpressure Algorithm

BP routing and scheduling consist of 4 steps, as illustrated in the block at the lower left of Fig. 2. In step 1, the optimal commodity $c_{ij}^*(t)$ on each directed link $(\overrightarrow{i,j})$ is selected as the one with the maximal backpressure,

$$c_{ij}^*(t) = \operatorname{argmax}_{c \in \mathcal{V}} \{U_i^{(c)}(t) - U_j^{(c)}(t)\}, \quad (1)$$

where $U_i^{(c)}(t)$ is the backlog metric, whose relationship with queue lengths is detailed in Section III-C. For shorter notation, we define the backpressure of commodity c on the directed link $(\overrightarrow{i,j})$ as $U_{ij}^{(c)}(t) = U_i^{(c)}(t) - U_j^{(c)}(t)$. In step 2, the maximum backpressure of $(\overrightarrow{i,j})$ is found as:

$$w_{ij}(t) = \max \left\{ U_i^{(c_{ij}^*(t))}(t) - U_j^{(c_{ij}^*(t))}(t), 0 \right\}. \quad (2)$$

In step 3, MaxWeight scheduling [3] finds the schedule $\mathbf{s}(t) \in \{0, 1\}^{|\mathcal{E}|}$ to activate a set of *non-conflicting links* achieving the maximum total utility,

$$\mathbf{s}(t) = \operatorname{argmax}_{\mathbf{s}(t) \in \mathcal{S}} \tilde{\mathbf{s}}(t)^\top [\mathbf{R}_{*,t} \odot \tilde{\mathbf{w}}(t)], \quad (3)$$

where vector $\mathbf{R}_{*,t}$ collects the real-time link rate of all links, vector $\tilde{\mathbf{w}}(t) = [\tilde{w}_{ij}(t) | (i,j) \in \mathcal{E}]$, and $\tilde{w}_{ij} = \max\{w_{ij}(t), w_{ji}(t)\} \cdot \mathbb{1}[Q_i^{(c_{ij}^*(t))}(t) > 0]$, and the direction of the link selected by the max function will be recorded for step 4. In (3), \mathcal{S} denotes the set of all non-conflicting configurations, and the per-link utility is $u_{ij}(t) = \mathbf{R}_{ij,t} \tilde{w}_{ij}(t)$. MaxWeight scheduling involves solving an NP-hard maximum weighted independent set (MWIS) problem [53] on the conflict graph to find a set of non-conflicting links. In practice, (3) can be solved approximately by distributed heuristics, such as local greedy scheduler (LGS) [28] and its GCN-based enhancement [44]. In step 4, all of the real-time link rate $\mathbf{R}_{ij,t}$ of a scheduled link is allocated to its optimal commodity $c_{ij}^*(t)$. The final transmission and routing variables of commodity $c \in \mathcal{V}$ on link $(\overrightarrow{i,j})$ is

$$\mu_{ij}^{(c)}(t) = \begin{cases} \mathbf{R}_{ij,t}, & \text{if } c = c_{ij}^*(t), w_{ij}(t) > 0, s_{ij}(t) = 1, \\ 0, & \text{otherwise.} \end{cases} \quad (4)$$

C. (Biased) Backlog Metrics

The queue length of commodity $c \in \mathcal{V}$ on node $i \in \mathcal{V}$ evolves as follows:

$$Q_i^{(c)}(t+1) = \max \left[Q_i^{(c)}(t) - M_{i-}^{(c)}(t), 0 \right] + M_{i+}^{(c)}(t) + A_i^{(c)}(t), \quad (5)$$

where $M_{i-}^{(c)}(t) = \sum_{j \in \mathcal{V}} \mu_{ij}^{(c)}(t)$ and $M_{i+}^{(c)}(t) = \sum_{j \in \mathcal{V}} \mu_{ji}^{(c)}(t)$ are the numbers of packets of commodity c respectively

transmitted and received by node i at time t ; $A_i^{(c)}(t)$ is the number of external packets of commodity c injected into node i at time t . We assume that the injection follows a random process with an arrival rate $\lambda_i^{(c)} = \mathbb{E}[A_i^{(c)}(t)]$ at source nodes, otherwise it is zero.

The general form of the backlog metric, i.e., $U_i^{(c)}(t)$ in (1), in low-overhead BP schemes can be expressed as

$$U_i^{(c)}(t) = g \left(\mathcal{Q}_i^{(c)}(t) \right) + B_i^{(c)}, \quad (6)$$

where $g(\cdot)$ is a function of QSI, and $0 \leq B_i^{(c)} < \infty$ is a queue-agnostic bias. In queue length-based BP, $g(\mathcal{Q}_i^{(c)}(t)) = Q_i^{(c)}(t)$, whereas in delay-based BP, $g(\mathcal{Q}_i^{(c)}(t))$ can be the sojourn time of the head-of-line (HOL) packet [19] or the entire queue, i.e., sojourn time backlog (SJB) [21].

In unbiased BP, including the basic and delay-based BP, $B_i^{(c)} = 0$. In biased BP [1], [12], [13], [15], $B_i^{(c)} \geq 0$ is defined based on the shortest path distance between node i and destination c . The matrix of all biases is denoted as $\mathbf{B} = (B_i^{(c)})$ for all $i, c \in \mathcal{V}$. The shortest path distances can be computed by distributed algorithms for single source shortest path (SSSP) or all pairs shortest path (APSP) on a given network topology, as illustrated in the middle of Fig. 2.

IV. LINK DUTY CYCLE PREDICTION WITH GNNs

Existing SP-BP algorithms are based on the hop distance (minimal hop count) between two nodes in the networks, which implicitly assumes that every link contributes equally to the end-to-end delay of routing. This, however, ignores the fact that the average delay of each link is different due to its network locality and link scheduling policy. In MaxWeight scheduling, the likelihood of a link being scheduled depends on its local conflict or interference topology and the network traffic load. We propose using a graph convolutional neural network (GCNN) to predict the expected delay on each link, which can serve to design a shortest path bias between node i and the destination node c in (6) better than the shortest hop distance. The GNN and its training setup are illustrated in the upper right blocks of Fig. 2, while the optimal scaling of link weights is discussed in Section V-A. Since our focus is on model-based framework that enables the applications of GNNs for enhancing SP-BP, we select GCNN for its simplicity and good generalizability, leaving the search of optimal GNN architectures and hyperparameters for the future work.

A. Graph Convolutional Neural Networks

We propose to predict the link duty cycle $\mathbf{x} \in \mathbb{R}^{|\mathcal{E}|}$, as $\mathbf{x} = \Psi_{\mathcal{G}^c}(\mathbf{1}; \boldsymbol{\omega})$, where $\Psi_{\mathcal{G}^c}$ is an L -layered featureless GCNN defined on the conflict graph \mathcal{G}^c , with a collection of trainable parameters $\boldsymbol{\omega}$. We define the output of an intermediate l -th layer of the GCNN as $\mathbf{X}^l \in \mathbb{R}^{|\mathcal{E}| \times g_l}$, $\mathbf{X}^0 = \mathbf{1}^{|\mathcal{E}| \times 1}$, $\mathbf{x} = \mathbf{X}_{*1}^L$ (the first column of \mathbf{X}^L), and the l -th layer of the GCNN is expressed as

$$\mathbf{X}^l = \sigma_l \left(\mathbf{X}^{l-1} \boldsymbol{\Theta}_0^l + \mathcal{L} \mathbf{X}^{l-1} \boldsymbol{\Theta}_1^l \right), \quad l \in \{1, \dots, L\}. \quad (7)$$

In (7), \mathcal{L} is the normalized Laplacian of \mathcal{G}^c , $\boldsymbol{\Theta}_0^l, \boldsymbol{\Theta}_1^l \in \mathbb{R}^{g_{l-1} \times g_l}$ are trainable parameters (collected in $\boldsymbol{\omega}$), and $\sigma_l(\cdot)$ is

the activation function of the l -th layer. The input and output dimensions are set as $g_0 = 1$ and $g_L = 2$. The activation functions of the input and hidden layers are selected as leaky ReLUs, whereas a node-wise softmax activation is applied at the output layer (each row of \mathbf{X}^L). This design limits the scale of output \mathbf{x} regardless of the density of input graph \mathcal{G}^c . Since \mathcal{L} in (7) is a local operator on \mathcal{G}^c , each row of \mathbf{X}^l , e.g., $\mathbf{X}_{e*}^l, e \in \mathcal{E}$ can be computed through neighborhood aggregation as the following local operation on link e ,

$$\mathbf{X}_{e*}^l = \sigma_l \left(\mathbf{X}_{e*}^{l-1} \Theta_0^l + \left[\mathbf{X}_{e*}^{l-1} - \sum_{u \in \mathcal{N}_{\mathcal{G}^c}(e)} \frac{\mathbf{X}_{u*}^{l-1}}{\sqrt{d(e)d(u)}} \right] \Theta_1^l \right), \quad (8)$$

where $\mathbf{X}_{e*}^l \in \mathbb{R}^{1 \times g_l}$ captures the l th-layer features on e , $\mathcal{N}_{\mathcal{G}^c}(e)$ denotes the set of (interfering) neighbors of e , and $d(\cdot)$ is the degree of a vertex in \mathcal{G}^c . Based on (8), the link duty cycle vector \mathbf{x} can be computed in a fully distributed manner through L rounds of local message exchanges between $e \in \mathcal{E}$ and its neighbors, making our delay-enhanced BP routing a distributed algorithm.

B. Delay-Aware Edge Weights

Depending on the availability of the long-term link rate r_e and link duty cycle x_e for any link $e \in \mathcal{E}$, we consider the weight of each link for finding the shortest path distance between any pair of nodes to be defined in three possible ways: $\delta_e = 1/x_e$, $\delta_e = 1/r_e$, or $\delta_e = \bar{r}/(x_e r_e)$, where \bar{r} is the network-wide average link rate defined in Section III-A. In addition, these link weights can be optimally scaled by \bar{r}/δ_{\min} based on the principle in Section V-A. The computation of vector $\boldsymbol{\delta} = [\delta_e | e \in \mathcal{E}]$ is denoted as a function $\boldsymbol{\delta} = f_w(\mathbf{x}, \mathbf{r}, \bar{r})$. By setting the edge weights of the connectivity graph \mathcal{G}^n as $\boldsymbol{\delta}$, bias $B_i^{(c)}$ is set as the *weighted* shortest path distance between nodes i and c on \mathcal{G}^n . This distance can be computed with distributed algorithms, such as weighted APSP in general or weighted SSSP when a new node joins the network.

C. Complexity

For distributed implementation, the local communication complexity (defined as the rounds of local exchanges between a node and its neighbors) of the GNN is $\mathcal{O}(L)$. On weighted graphs, the distributed SSSP with the Bellman-Ford algorithm [54], [55] and state-of-the-art APSP [56] both take $\mathcal{O}(|\mathcal{V}|)$ rounds. On unweighted graphs, the distributed SSSP and APSP take $\mathcal{O}(D)$ and $\mathcal{O}(|\mathcal{V}|)$ rounds, respectively, where D is the diameter of the unweighted \mathcal{G}^n . Compared to the hop distance-based methods [12], [13], our approach bears additional $\mathcal{O}(L)$ rounds of communications (and larger message size). Notice that the bias matrix \mathbf{B} can be reused over time slots until the network topology (\mathcal{G}^n or \mathcal{G}^c) changes, which is critical for overhead reduction and scalability promotion.

D. Training

The parameters $\boldsymbol{\omega}$ (collecting Θ_0^l and Θ_1^l across all layers l) of our GNN are trained on a set of routing instances defined on random network processes drawn from a target

Algorithm 1 Pseudo-code for a training or testing instance

Input: $\mathcal{G}^n, \mathcal{G}^c, \mathcal{F}, \mathbf{A}, \mathbf{R}, T; \boldsymbol{\omega}$, training
Output: performance metrics, $\boldsymbol{\omega}$ (for training only)

- 1: $r_e = \mathbb{E}_{t \leq T} [\mathbf{R}_{e,t}]$ for all $e \in \mathcal{E}$; $\bar{r} = \mathbb{E}_{e \in \mathcal{E}, t \leq T} [\mathbf{R}_{e,t}]$
- 2: $\mathbf{x} = \Psi_{\mathcal{G}^c}(\mathbf{1}; \boldsymbol{\omega}), \boldsymbol{\delta} = f_w(\mathbf{x}, \mathbf{r}, \bar{r})$
- 3: Compute \mathbf{B} from $(\mathcal{G}^n, \boldsymbol{\delta})$ using APSP
- 4: $\mathcal{Q}_i^{(c)}(0) = \phi$, for all $i, c \in \mathcal{V}$ (ϕ : empty set)
- 5: $\mathcal{M} = \phi; t = 0$
- 6: **while** $t < T$ **do**
- 7: **for all** $i \in \mathcal{V}'$ **do**
- 8: Compute $U_i^{(c)}(t)$ based on (6)
- 9: Compute $c_{ij}^*(t)$ for all $j \in \mathcal{N}(i)$ based on (1)
- 10: Compute $w_{ij}(t)$ for all $j \in \mathcal{N}(i)$ based on (2)
- 11: Compute $\mathbf{s}(t)$ with MaxWeight scheduling in (3)
- 12: Compute $\{\mu_{ij}^{(c)}(t) | i, j, c \in \mathcal{V}\}$ based on (4)
- 13: **end for**
- 14: Queueing state evolution: update $\{\mathcal{Q}_i^{(c)}(t+1) | i, c \in \mathcal{V}\}$ based on $\{\mathcal{Q}_i^{(c)}(t)\}, \mathbf{A}_{*t}, \mathbf{R}_{*t}$, and $\{\mu_{ij}^{(c)}(t)\}$
- 15: **if** training **then**
- 16: $\mathcal{M} \leftarrow \mathcal{M} \cup \{\nabla_{\boldsymbol{\omega}} \ell(\boldsymbol{\omega})\}$
- 17: **end if**
- 18: **end while**
- 19: Collect performance metrics
- 20: **if** training **then**
- 21: Update $\boldsymbol{\omega}$ based on gradient buffer \mathcal{M} with optimizer
- 22: **end if**

distribution Ω . More precisely, we draw several instances (indexed by k) of the network topology, flows, packet arrivals, and link rates $(\mathcal{G}^n(k), \mathcal{G}^c(k), \mathcal{F}(k), \mathbf{A}(k), \mathbf{R}(k)) \sim \Omega$. For every instance, the training or testing procedure is detailed in Algorithm 1 and explained as follows: the GNN first predicts the link duty cycle vector $\mathbf{x}(k) = \Psi_{\mathcal{G}^c(k)}(\mathbf{1}; \boldsymbol{\omega})$, then biases $\mathbf{B}(k)$ are generated by the APSP algorithm based on the link distance vector $\boldsymbol{\delta}(k) = \text{diag}^{-1}(\mathbf{x}(k))\mathbf{1}$, then we run the bias-based backpressure routing for T time slots, and collect the schedules for each time slot, $\mathbf{s}^k(t)$, with the employed LGS scheduler [28]. As indicated by the blue modules in Fig. 2, we train the parameters $\boldsymbol{\omega}$ of GNN to minimize the following mean squared error loss

$$\ell(\boldsymbol{\omega}) = \mathbb{E}_{\Omega} \left\{ \frac{1}{|\mathcal{E}|} \left\| \mathbf{X}^L(k) - \frac{1}{T} \sum_{t=1}^T [\mathbf{s}^k(t), \mathbf{1} - \mathbf{s}^k(t)] \right\|_2^2 \right\}. \quad (9)$$

Intuitively, by minimizing the loss in (9), we are choosing parameters $\boldsymbol{\omega}$ such that the softmax output of our GNN \mathbf{X}^L is close to predicting the fraction of time that each link is scheduled. We do not seek to learn this complex function for *any specific* topology, but rather, we want to minimize the average error over instances drawn from Ω . In practice, we approximate the expected values in (9) with the corresponding empirical averages. Indeed, with the collected experience tuples, we update the parameters $\boldsymbol{\omega}$ of the GNN after each training instance, through batch training with random memory sampling, employing the Adam optimizer. Notice that, once trained, the GNN can be used to compute the delay-aware bias for previously unseen topologies without any retraining.

As long as the new topology, arrival rates, and link rates are similar to those observed in Ω during training, we illustrate in Section VII that the trained GCNN generalizes to new test instances not observed during training.

V. IMPROVEMENTS TO BIASED BACKPRESSURE

To further improve the latency and practicality of SP-BP schemes, we propose three additional enhancements.

A. Optimal Scaling of Edge Weights

To the best of our knowledge, the constant scale of the edge weights $\delta_e, e \in \mathcal{E}$ for computing the shortest path biases in SP-BP schemes are often selected via trial-and-error, such as a constant δ_e for all $e \in \mathcal{E}$ in EDR [12] and $\delta_e = \bar{r}/(x_e r_e)$ proposed in Section IV-B. Our goal is to provide a principled method of optimization for such scaling parameter(s).

For biased BP with low-to-medium traffic loads, including the last packets situation, a key observation is that bias scaling influences the random walk behaviors of packets and subsequently the end-to-end delay. Consider an exemplary situation of last packets in BP routing with only one commodity (flow), for which the queueing states of four nodes in two consecutive time steps are illustrated in Fig. 3. The hop distances of nodes A, B, C, D to the destination are $b+2, b+1, b+1, b$, respectively. Every link has a constant link rate of \bar{r} . At time t , $Q_A^{(c)}(t) = \bar{r}$ and $Q_B^{(c)}(t) = Q_C^{(c)}(t) = 0$, the backpressures point from A towards B and C . Assume that at the beginning of time slot $t+1$, all the packets on A moved to B . Different choices of δ_e would lead to different routing decisions at $t+1$.

For unbiased BP with $\delta_e = 0$, the backpressures (orange arrows) are pointed from B towards A, C , and D , and $U_{BA}^{(c)}(t+1) = U_{BC}^{(c)}(t+1) = \bar{r} > U_{BD}^{(c)}(t+1)$. At the end of time slot $t+1$, the packets on B will move to either A or C , packets on D may also move back to C , causing an unwanted meandering of the packets. For biased BP with $\delta_e > 0$, the backpressures (magenta and green arrows) at time $t+1$ originating from B are skewed towards the destination, $U_{BD}^{(c)}(t+1) > U_{BC}^{(c)}(t+1) = \bar{r} > U_{BA}^{(c)}(t+1)$. At the end of time slot $t+1$, packets in B will move forward to D . In particular, when $\delta_e = \bar{r}$, the backpressure (i.e., green arrows) $U_{BA}^{(c)}(t+1) = 0$.

The previous example can be formally described as follows. Consider a wireless multi-hop network with homogeneous link rates, i.e., all links have a link rate of \bar{r} , there are two links (i, j) and (j, k) , where nodes j, k are on the shortest path from node i to node c . Further, consider a congestion-free last packets (CFLP) scenario: at time t , the last packets of commodity c reside on node i , and link (i, j) is congestion-free, i.e., $0 < Q_i^{(c)}(t) = q \leq \bar{r}, Q_j^{(c)}(t) = 0$ and no external packets of commodity c will arrive at nodes i, j, k from the rest of the network or users. If link (i, j) is scheduled at time t , such that $Q_i^{(c)}(t+1) = 0, Q_j^{(c)}(t+1) = q \leq \bar{r}$, we have the following Lemma.

Lemma 1. *In SP-BP routing under the CFLP scenario, the edge weight δ_e should be greater than or equal to the homogeneous link rate, $\delta_e \geq \bar{r}$, to avoid the immediate*

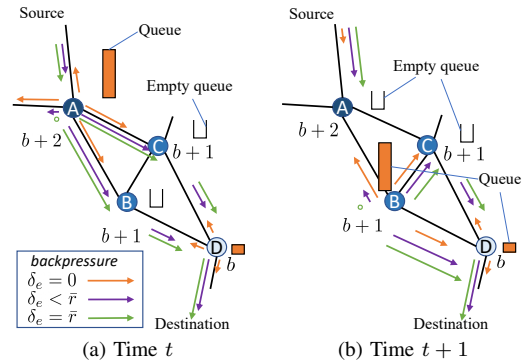


Fig. 3: The queue states at four nodes (with hop distance to the destination marked) in an exemplary case of backpressure routing with a single commodity, at time (a) t and (b) $t+1$. An arrow indicates the magnitude and direction of pressure on a link, and its color encodes the choice of the edge weight. All links have an identical \bar{r} rate.

reversal of the direction of backpressure for commodity c on the scheduled link (i, j) after the transmission.

Proof. In queue length-based SP-BP, the backpressure on link (i, j) is $U_{ij}^{(c)}(t) = Q_{ij}^{(c)}(t) + (B_i^{(c)} - B_j^{(c)}) = q + \delta_e$. Since link (i, j) is scheduled at time t , we have that $U_{ij}^{(c)}(t+1) = \delta_e - q$. To avoid the direction of the backpressure on link (i, j) being reversed at time $t+1$, i.e., $U_{ij}^{(c)}(t+1) < 0$, we need to set $\delta_e \geq \bar{r}$. \square

In the described CFLP scenario, Lemma 1 ensures that the backpressure algorithm does not oscillate as the last packets travel through the shortest path when $\delta_e \geq \bar{r}$. On the other hand, a smaller value of δ_e is preferable for path finding and congestion prevention. Indeed, an extremely large SP bias scaling δ_e would force every packet through the shortest path, thus hindering any information from the queue lengths and defeating the original purpose of BP routing. Combining these two observations, we advocate for setting the minimal edge weight as the average link rate, i.e., $\min_{e \in \mathcal{E}} \delta_e := \bar{r}$. In particular, for EDR in [12], this implies setting $\delta_e = \bar{r}$.

Although the above discussion is based on the CFLP setting with all link rates equal to the average \bar{r} , in Section VII, we demonstrate experimentally the optimality of the above choice under heterogeneous link rates and general traffic settings.

B. Bias Maintenance

Due to the mobility and distributed nature of networks, bias maintenance requires frequent or periodical SSSP and/or APSP computation. Although the biases \mathbf{B} can be re-used for many time slots to match the slowly changing topology, the overhead of bias maintenance can be high for large networks.

To address this issue, we propose to adopt the neighborhood update rule from Dijkstra's algorithm [57] for bias maintenance at node $i \in \mathcal{V}$, whenever one or more of its incident links are established or destroyed

$$B_i^{(c)}(t+1) = \begin{cases} \min_{j \in \mathcal{N}_{\mathcal{G}^n}(i)} [B_j^{(c)}(t) + \delta_{ij}(t)], & i \neq c \\ 0, & i = c \end{cases}, \quad (10)$$

where $\delta_{ij}(t)$ is the edge weight between neighboring nodes i and j . This rule allows the shortest path bias to be updated within $\mathcal{O}(D)$ steps of local message exchange.

C. Delay-aware backlog metric: $\exp Q$

To prioritize old packets, we further introduce a SP-BP-friendly delay-aware QSI function $g(\cdot)$ in (6):

$$g(Q_i^{(c)}(t+1)) = (1+\epsilon)g(Q_i^{(c)}(t)) \max \left[1 - \frac{M_{i-}^{(c)}(t)}{Q_i^{(c)}(t)}, 0 \right] + M_{i+}^{(c)}(t) + A_i^{(c)}(t), \quad (11)$$

where $\epsilon \geq 0$ is a small constant parameter, and it follows that $g(Q_i^{(c)}(t)) = Q_i^{(c)}(t)$ for $\epsilon = 0$ and that $g(\emptyset) = 0$ for an empty queue \emptyset . With this definition, it is easy to find that $g(Q_i^{(c)}(t)) \geq Q_i^{(c)}(t)$. Further restrictions on ϵ can be found in (25) and the following discussion in Section VI-B.

The $g(\cdot)$ in (11) is named $\exp Q$, as it will increase exponentially over time if commodity c at node i is not scheduled. Compared to the backpressure metric based on sojourn time backlog [21] and HOL sojourn time [19], $\exp Q$ can increase the bandwidth utilization efficiency, since it does not require tracking the sojourn time of individual packets.

VI. THROUGHPUT OPTIMALITY

The throughput optimality of a routing scheme states that all queues in the network are strongly stable as long as the arrival rates of flows are within the network capacity region. The condition of strong stability is defined as [12]–[15]

$$\limsup_{t \rightarrow \infty} \frac{1}{t} \sum_{\tau=0}^{t-1} \mathbb{E} [Q_i^{(c)}(\tau)] < \infty, \text{ for all } i, c \in \mathcal{V}. \quad (12)$$

Next, we first prove the throughput optimality of queue length-based SP-BP through Lyapunov drift theory [12]–[15], then the conditional throughput optimality for SP-BP with $\exp Q$.

A. Queue length-based SP-BP scheme

Our proof is similar to [12]–[15], except for (15)–(17).

Theorem 1. A SP-BP scheme with backlog metric, $U_i^{(c)}(t) = Q_i^{(c)}(t) + B_i^{(c)}$ for all $i, c \in \mathcal{V}$, where $0 \leq B_i^{(c)} < \infty$ is a non-negative queue-agnostic constant bias, meets the condition of strong stability in (12) within the network capacity region.

Proof. Define $\mathbf{Q}(t) = (Q_i^{(c)}(t))_{i,c \in \mathcal{V}}$ as the current queueing state of the network. Define the Lyapunov function as

$$L(t) := \frac{1}{2} \sum_{i \in \mathcal{V}} \sum_{c \in \mathcal{V}} U_i^{(c)}(t)^2, \quad (13)$$

and the Lyapunov drift as

$$\Delta(t) := \mathbb{E} [L(t+1) - L(t) | \mathbf{Q}(t)]. \quad (14)$$

The evolution of metric $U_i^{(c)}(t) = Q_i^{(c)}(t) + B_i^{(c)}$ follows

$$U_i^{(c)}(t+1) = \max [U_i^{(c)}(t) - M_{i-}^{(c)}(t), B_i^{(c)}] + M_{i+}^{(c)}(t) + A_i^{(c)}(t). \quad (15)$$

By squaring the queue update in (15), and using the fact that $(\max[q - o, b] + p)^2 \leq q^2 + o^2 + p^2 + b^2 + 2bp + 2q(p - o)$ for $q \geq 0, o \geq 0, b \geq 0, p \geq 0$ (see Appendix A), we have:

$$\Delta(t) \leq W + \sum_{i,c \in \mathcal{V}} U_i^{(c)}(t) \mathbb{E} [\lambda_i^{(c)} + M_{i+}^{(c)}(t) - M_{i-}^{(c)}(t) | \mathbf{Q}(t)], \quad (16)$$

where $\mathbb{E} [A_i^{(c)}(t) | \mathbf{Q}(t)] = \lambda_i^{(c)}$ and W is a finite constant that depends on the maximum possible first and second moments of packet arrival rates and transmission rates:

$$W \geq \frac{1}{2} \sum_{i,c \in \mathcal{V}} \mathbb{E} \left\{ \left[M_{i-}^{(c)}(t) \right]^2 + \left[M_{i+}^{(c)}(t) + A_i^{(c)}(t) \right]^2 + \left[B_i^{(c)} \right]^2 + 2B_i^{(c)} \left[M_{i+}^{(c)}(t) + \lambda_i^{(c)} \right] \right\}. \quad (17)$$

Next, we show that the biased BP described in Section III-B is designed to choose a feasible policy $\mathbf{M}(t) = (\mu_{ij}^{(c)}(t))_{i,j,c \in \mathcal{V}}$ under current network state to minimize the bound of the Lyapunov drift, i.e., the right-hand side of (16). Since W and $\lambda_i^{(c)}$ are constants, this amounts to minimizing the following:

$$\mathbb{E} \left\{ \sum_{i,c \in \mathcal{V}} U_i^{(c)}(t) \left[M_{i+}^{(c)}(t) - M_{i-}^{(c)}(t) \right] \middle| \mathbf{Q}(t) \right\},$$

where the finite sums in the second term in (16) are pushed through the expectations. By the principle of opportunistically minimizing an expectation, we can minimize the above expectation by minimizing the function inside of it given the observed $\mathbf{Q}(t)$ and network topology (network state):

$$\mathbf{M}^*(t) = \underset{\mathbf{M}(t) \in \Pi}{\operatorname{argmin}} \sum_{i,c \in \mathcal{V}} U_i^{(c)}(t) \left[\sum_{j \in \mathcal{V}} \mu_{ji}^{(c)}(t) - \sum_{j \in \mathcal{V}} \mu_{ij}^{(c)}(t) \right], \quad (18)$$

where Π is the feasible policy space of routing and scheduling decisions. By rearranging the sums in (18), we have

$$\mathbf{M}^*(t) = \underset{\mathbf{M}(t) \in \Pi}{\operatorname{argmax}} \sum_{i \in \mathcal{V}} \sum_{j \in \mathcal{V}} \sum_{c \in \mathcal{V}} \mu_{ij}^{(c)} \left[U_i^{(c)}(t) - U_j^{(c)}(t) \right]. \quad (19)$$

Notice that (19) is equivalent to SP-BP in (1)–(4). Since the bound on the Lyapunov drift in (16) is minimized, the arrival rates within the network capacity region $(\lambda_i^{(c)})_{i,c \in \mathcal{V}} \in \Lambda$ can be expressed as that there is a constant $\beta > 0$ such that

$$\mathbb{E} [\lambda_i^{(c)} + M_{i+}^{(c)}(t) - M_{i-}^{(c)}(t) | \mathbf{Q}(t)] \leq -\beta, \text{ for all } i, c \in \mathcal{V}.$$

Substituting the expectation in (16) with $-\beta$, we have

$$\Delta(t) \leq W - \beta \sum_{i,c \in \mathcal{V}} U_i^{(c)}(t). \quad (20)$$

The time average of (20) yields [13, Lemma 4.1]:

$$\limsup_{t \rightarrow \infty} \frac{1}{t} \sum_{\tau=0}^{t-1} \sum_{i,c \in \mathcal{V}} \mathbb{E} [Q_i^{(c)}(\tau) + B_i^{(c)}] < \frac{W}{\beta}. \quad (21)$$

Since $W < \infty$, $0 \leq B_i^{(c)} < \infty$, the condition of strong stability in (12) immediately follows by moving $\sum_{i,c \in \mathcal{V}} B_i^{(c)}$ from the left hand side of (21) to the right hand side. \square

B. SP-BP scheme with $\exp Q$

Theorem 2. *There exists a constant $\epsilon \geq 0$ such that SP-BP with delay-based backlog metric $\exp Q$ defined in Section V-C, denoted as $E_i^{(c)}(t) = g(Q_i^{(c)}(t))$, meets the condition of strong stability in (12) within a reduced network capacity region.*

Proof. We denote the backlog metric of SP-BP with $\exp Q$ as $\tilde{U}_i^{(c)}(t) = E_i^{(c)}(t) + B_i^{(c)}$, and consider the compounding component of $E_i^{(c)}(t)$ in (11) as virtual packet arrivals, which is assumed to be bounded for a finite $t < \infty$ and some $\epsilon \geq 0$:

$$\epsilon E_i^{(c)}(t) \max \left[1 - \frac{M_i^{(c)}(t)}{Q_i^{(c)}(t)}, 0 \right] \leq \epsilon E_i^{(c)}(t) \leq b.$$

This, along with (11) and $E_i^{(c)}(t) \geq Q_i^{(c)}(t)$, lead to

$$\tilde{U}_i^{(c)}(t+1) \leq \max \left[\tilde{U}_i^{(c)}(t) - M_{i-}^{(c)}(t), B_i^{(c)} \right] + M_{i+}^{(c)}(t) + A_i^{(c)}(t) + b. \quad (22)$$

We apply the proof for Theorem 1 by substituting (15) with (22), and replacing $U_i^{(c)}(t)$ by $\tilde{U}_i^{(c)}(t)$ and $A_i^{(c)}(t)$ by $A_i^{(c)}(t) + b$, thus obtain the policy of SP-BP with $\exp Q$ as

$$\mathbf{M}^*(t) = \operatorname{argmax}_{\mathbf{M}(t) \in \Pi} \sum_{i \in \mathcal{V}} \sum_{j \in \mathcal{V}} \sum_{c \in \mathcal{V}} \mu_{ij}^{(c)} \left[\tilde{U}_i^{(c)}(t) - \tilde{U}_j^{(c)}(t) \right], \quad (23)$$

and that within a reduced capacity region $(\lambda_i^{(c)} + b)_{i,c \in \mathcal{V}} \in \Lambda$, there is a constant $\beta > 0$ such that for all $i, c \in \mathcal{V}$

$$\mathbb{E} \left[\lambda_i^{(c)} + b + M_{i+}^{(c)}(t) - M_{i-}^{(c)}(t) \middle| \mathbf{Q}(t) \right] \leq -\beta.$$

Subsequently, $\exp Q$ meets the condition of strong stability

$$\limsup_{t \rightarrow \infty} \frac{1}{t} \sum_{\tau=0}^{t-1} \sum_{i,c \in \mathcal{V}} \mathbb{E} \left[E_i^{(c)}(\tau) \right] < \frac{W}{\beta} - \sum_{i,c \in \mathcal{V}} B_i^{(c)}. \quad (24)$$

With $E_i^{(c)}(0) < \infty$ and $|E_i^{(c)}(t+1) - E_i^{(c)}(t)| < \infty$, (24) leads to uniform boundness $E_i^{(c)}(t) < \gamma < \infty$. The condition for the above process to be true for $t \rightarrow \infty$ is

$$0 \leq \epsilon \leq \frac{b}{\gamma}, \text{ where } (\lambda_i^{(c)} + b)_{i,c \in \mathcal{V}} \in \Lambda, E_i^{(c)}(t) < \gamma. \quad (25)$$

With (24), (25) and $E_i^{(c)}(t) \geq Q_i^{(c)}(t)$, all queues are strongly stable within the network capacity region shrank by b . \square

According to (25), in order to come up with a reasonable ϵ for $\exp Q$, we need an allowable reduction of capacity region, b , and an estimated upper bound of $E_i^{(c)}(t)$.

Simulations in [13, Ch 4.9] and Section VII-C show that for BP with queue length-based backlog metrics, the inclusion of non-negative queue-agnostic biases does not shrink the network capacity region of the basic BP. However, as illustrated in Section VII-C, the application of delay-based backlog metrics, including $\exp Q$, will reduce the network capacity of BP.

VII. NUMERICAL EXPERIMENTS

To illustrate the effectiveness of our proposed enhancements to the SP-BP schemes in improving routing performance, we evaluate a series of low-overhead BP routing algorithms in simulated wireless multi-hop networks. Each network instance is generated by a 2D point process with a given number of

TABLE I: Hyperparameters for Training

Item	Value
GCNN config	$L = 5, g_l = 32$ for $1 \leq l \leq 4, g_0 = 1, g_L = 2$, see Section IV-A for other details
Regularization	L2 regularization with a weight decay of 0.001
Learning rate	0.0001
Simulation steps	$T = 200$ per training instance
Mini-batch size	1 training instance
Training graphs	A set of 5000 random networks, with size $ \mathcal{V} \in \{20, 30, 40, 50, 60\}$, 100 instances per $ \mathcal{V} $
Interference radius	Uniformly random $\mathbb{U}(0, 0.8)$
Link rates	Same as test setting
Number of flows	Uniformly chosen between $\lfloor 0.15 \mathcal{V} \rfloor$ and $\lceil 0.30 \mathcal{V} \rceil$
Traffic pattern	All streaming flows with $\lambda(f) \sim \mathbb{U}(0.2, 1.0)$

nodes $|\mathcal{V}| \in \{20, 30, \dots, 110\}$ uniformly distributed in the plane with a constant density of $8/\pi$. We consider a simplified scenario where all mobile devices are equipped with omnidirectional antennas and transmit at identical power levels, which can be captured by the unit-disk interference model previewed in Section III-A. A link is established between two nodes if they are located within a distance of 1 unit. The average degree of conflict graphs under this test configuration is 34.6. For each network size $|\mathcal{V}|$, we generate 100 test instances by drawing 10 instances of random networks, each with 10 realizations of random source-destination pairs and random link rates. A test instance contains a number (uniformly chosen between $\lfloor 0.30|\mathcal{V}| \rfloor$ and $\lceil 0.50|\mathcal{V}| \rceil$) of random flows between different pairs of sources and destinations. Each test instance also includes a realization of uniformly distributed long-term link rates, $r_e \sim \mathbb{U}(10, 42)$, which are the expected values of the real-time link rates, $\mathbf{R}_{e,t} \sim \mathbb{N}(r_e, 3)$, truncated to between $r_e \pm 9$. The link rates are configured to capture fading channels with lognormal shadowing. A test instance is simulated for a total of $T = 1000$ time steps.

Two types of flows are employed: in a *streaming* flow f , new packets arrive at the source following a Poisson process with a uniformly random arrival rate $\lambda(f) \sim \mathbb{U}(0.2, 1.0)$ for all time slots; in a *bursty* flow, packets follow Poisson arrivals with a random rate $\lambda(f) \sim \mathbb{U}(2.0, 10.0)$ (lighter traffic) or $\lambda(f) \sim \mathbb{U}(6.6, 33.0)$ (heavier traffic) for $t < 30$, and no new packet arrivals for $t \geq 30$. With $T = 1000$, a streaming and a heavier bursty flows are expected to inject similar total numbers of packets into the network, allowing better assessment of the impact of traffic pattern. These flow rates are considered lightweight since the expected exogenous packet arrival rate per node of 0.24 is only 8% of the expected total maximum outflow rate per node of 3, see Appendix B for details. The end-to-end delay of a tested BP scheme is collected by tracking the time each packet arrived at the source node t_0 and the destination node (departure time) t_1 . The end-to-end delay of an undelivered packet is treated as T . We record the latency of individual flows (source-destination pairs) by averaging the end-to-end delays of their packets.

We train a 5-layer GCNN ($L = 5, g_l = 32, l \in \{1, \dots, 4\}$) as detailed in Section IV-A according to the RL scheme in Section IV-D. The training instances are generated similar to the test instances described earlier, except that the underlying network instances are from a set of 100 random networks

TABLE II: Tested low-overhead BP algorithms and their detailed configurations, information requirements, and result summary.

SP-BP algorithm Acronym	Link Distance	Bias Scaling	Backlog $U_i^{(c)}(t)$	Local Info. [‡]	Global Info.	Means* (ranking) under streaming (s) & bursty (b) traffic				
						latency (s)	delivery (s)	latency (b)	delivery (b)	network capacity [†] (s)
BP	0	–	Q	–	–	891.1 (15)	12.9% (15)	870.1 (15)	14.7% (15)	32.83 (8)
BP-HOL	0	–	HOL	t_0	–	890.3 (14)	13.9% (14)	830.4 (14)	23.1% (14)	15.86 (15)
BP-SJB	0	–	SJB	t_0	–	874.1 (13)	16.1% (13)	792.8 (13)	26.9% (13)	29.89 (13)
EDR- \bar{r}	1	\bar{r}	Q	–	\bar{r}	196.7 (10)	88.1% (10)	245.3 (10)	92.1% (11)	49.45 (4)
EDR- \bar{r} -expQ	1	\bar{r}	Q	–	\bar{r}	194.3 (9)	89.2% (8)	227.0 (7)	96.6% (8)	30.95 (10)
EDR- \bar{r} -HOL	1	\bar{r}	HOL	t_0	\bar{r}	261.0 (11)	83.5% (11)	284.3 (11)	93.8% (9)	27.55 (14)
EDR- \bar{r} -SJB	1	\bar{r}	SJB	t_0	\bar{r}	804.2 (12)	24.3% (12)	713.5 (12)	38.0% (12)	30.04 (12)
SP-1/ x	1/ x	–	Q	x	–	187.8 (7)	88.9% (9)	240.5 (9)	92.8% (10)	49.33 (5)
SP-1/ x -expQ	1/ x	–	expQ	x	–	191.9 (8)	89.4% (7)	227.2 (8)	96.6% (7)	30.90 (10)
SP-1/ r -min	1/ r	$\bar{r}r_{\max}$	Q	r	\bar{r}, r_{\max}	90.0 (2)	96.3% (2)	169.9 (2)	98.7% (4)	54.43 (2)
SP-1/ r -min-expQ	1/ r	$\bar{r}r_{\max}$	expQ	r	\bar{r}, r_{\max}	115.6 (5)	95.0% (5)	176.4 (4)	99.1% (2)	37.71 (7)
SP- \bar{r} / (xr)	$\bar{r}/(xr)$	–	Q	r, x	\bar{r}	103.0 (3)	95.6% (3)	191.2 (5)	97.9% (6)	49.38 (3)
SP- \bar{r} / (xr) -expQ	$\bar{r}/(xr)$	–	expQ	r, x	\bar{r}	143.6 (6)	93.0% (6)	207.6 (6)	98.1% (5)	31.95 (9)
SP- \bar{r} / (xr) -min	$\bar{r}/(xr)$	$(xr)_{\max}$	Q	r, x	$\bar{r}, (xr)_{\max}$	88.7 (1)	96.4% (1)	166.9 (1)	98.8% (3)	55.26 (1)
SP- \bar{r} / (xr) -min-expQ	$\bar{r}/(xr)$	$(xr)_{\max}$	expQ	r, x	$\bar{r}, (xr)_{\max}$	111.3 (4)	95.2% (4)	171.4 (3)	99.2% (1)	38.82 (6)

t_0 : the time a packet arrives to the network, r : individual long-term link rate, \bar{r} : network average long-term link rate, x : predicted link duty cycle, Q : queue length, SJB: total sojourn time of all packets in a queue, HOL: sojourn time of head-of-line packet in a queue, $\text{exp}Q$: backlog function defined in (11).

‡ All the BP algorithms require instantaneous link rates $\mathbf{R}_{e,t}$ and conflicting degree $d(e)$ for $e \in \mathcal{E}$ in MaxWeight scheduling. Computing x_e requires $d(e)$.

* Latency and delivery rate based on mixed traffic; units: latency (number of time slots), network capacity (number of packets per time slot).

† Ranked by maximum network throughput on random networks of 100 nodes (Fig. 7); when maximal values are close, values for $\lambda \leq 3.0$ weigh in.

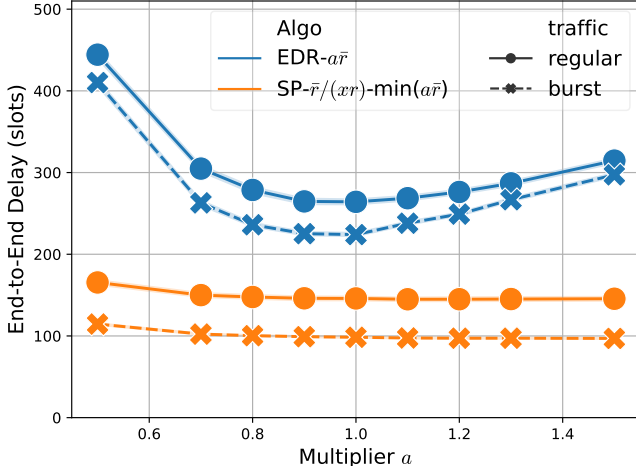


Fig. 4: End-to-end delay of SP-BP routing algorithms as a function of the multiplier of minimum edge weight $\min(\delta_e) = a\bar{r}$ on networks of 100 nodes, simulated with unit-disk interference model, long-term link rates $r_e \sim \mathbb{U}(10, 42)$, total time steps $T = 1000$, and 100 test instances per point. Flow rate $\lambda(f) \sim \mathbb{U}(0.2, 1.0)$ for streaming traffic, $\lambda(f) \sim \mathbb{U}(2.0, 10.0)$ for bursty traffic when $t < 30$.

with $|\mathcal{V}| \in \{20, 30, \dots, 60\}$, and the number of flows is uniformly chosen between $\lfloor 0.15|\mathcal{V}|\rfloor$ and $\lceil 0.30|\mathcal{V}|\rceil$. Notice that our test instances cover larger networks and denser traffic than our training configuration, to illustrate that our GNN-based SP-BP schemes can generalize to problems of larger scales. The detailed hyperparameters and training setting are listed in Table I, and the model converged after 5 epochs.¹

The tested BP algorithms (acronyms in parentheses identify legends in figures) include 1) unbiased BP: basic BP (BP), delay-based unbiased BP with SJB [21] (BP-SJB) and HOL [19] (BP-HOL); 2) queue-length based biased BP: EDR [12] with edge weight $\delta_e = \bar{r}$ (EDR- \bar{r}), and GCN-based delay-aware shortest path bias [1] (SP- \bar{r} / (xr)) with edge weight

¹Training takes 5 hours on a workstation with a specification of 32GB memory, 8 cores, and Geforce GTX 1070 GPU. The source code is published at <https://github.com/zhongyuanzhao/dutyBP>

$\delta_e = \bar{r}/(x_e r_e)$, and its scaled version (SP- \bar{r} / (xr) -min); and 3) delay-based biased BP: combination of BP-SJB and EDR- \bar{r} (EDR- \bar{r} -SJB), combination of BP-HOL and EDR- \bar{r} (EDR- \bar{r} -HOL), and the two biased BP schemes based on $\text{exp}Q$ (EDR- \bar{r} -expQ and SP- \bar{r} / (xr) -expQ) where $\epsilon = 0.01$ in (11). Postfix -min in legend refers to a SP-BP scheme with optimally scaled edge weight $\tilde{\delta}_e = \delta_e \bar{r} / (\min_{e \in \mathcal{E}} \delta_e)$. The details of these BP schemes, including their requirements on local and global information and test rankings, are listed in Table II.

A. Bias Scaling

We first examine the optimal bias scaling approach proposed in Section V-A. We test EDR- δ and SP- \bar{r} / (xr) -min with edge weight adjustment $\min_{e \in \mathcal{E}} \delta_e := a\bar{r}$, for $a \in [0.5, 1.5]$, on random networks of 100 nodes. The results in Fig. 4 show that $a = 1.0$ is indeed the optimal setting for EDR- δ and near-optimal setting for SP- \bar{r} / (xr) -min, under both streaming and bursty traffic. This provides empirical validation of the adjustment rule $\min_{e \in \mathcal{E}} \delta_e := \bar{r}$ advocated in Section V. Notice that the settings tested in Fig. 4 go beyond the simplified setting of CFLP with constant rates treated in Section V. However, the proposed scaling is still empirically optimal in these broader scenarios. Since SP- \bar{r} / (xr) -min can tolerate a wide range of a , to keep its distributed execution, it can be implemented based on statistical information of edge weights rather than their global minimum. The different sensitivities of the end-to-end delay to the scaling of edge weight under the two tested SP-BP schemes, as shown in Fig. 4, reveal that the shortest path based on link features [1] not only achieves better performance but is also more robust to the scaling choice.

B. Network Size and Traffic Type

Next, we evaluate various low-overhead BP algorithms in random networks of different sizes (20-110 nodes), presenting their performances in end-to-end delay and total packet

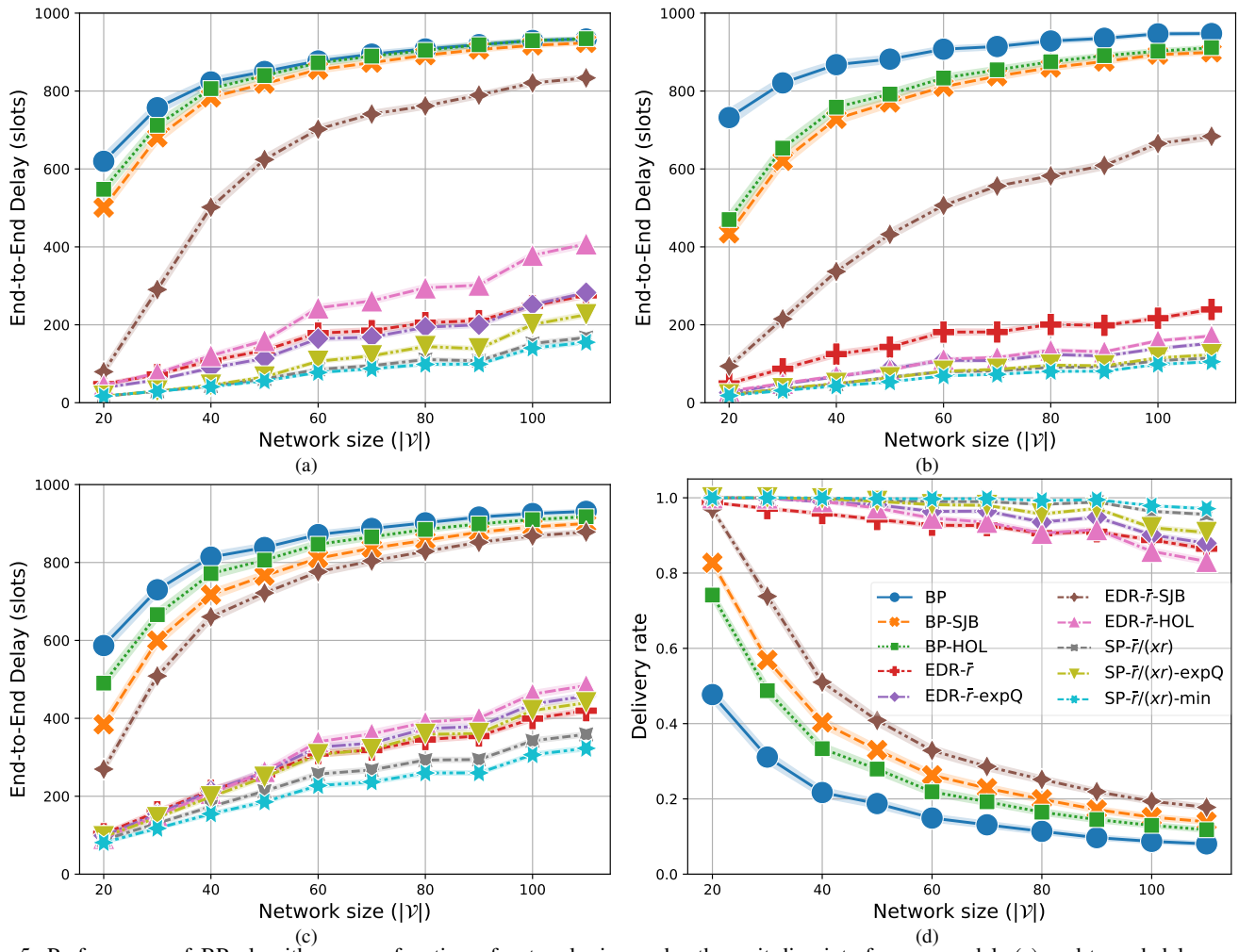


Fig. 5: Performance of BP algorithms as a function of network size under the unit-disc interference model: (a) end-to-end delay under streaming traffic, (b) end-to-end delay under bursty traffic with low flow rate $\lambda(f) \sim \mathbb{U}(2.0, 10.0)$ for $t < 30$, (c) end-to-end delay of bursty traffic with high flow rate $\lambda(f) \sim \mathbb{U}(6.6, 33.0)$ for $t < 30$, and (d) packet delivery rate of bursty traffic with high flow rate. Simulated with long-term link rates $r_e \sim \mathbb{U}(10, 42)$, total time steps $T = 1000$, and all queues are initialized to be empty. 100 test instances per point (10 random networks \times 10 realizations of random source-destination pairs and link rates). Error band indicates 95% confidence interval.

delivery rate after $T = 1000$ time steps. The evaluations are configured with three types of traffic: 1) all streaming flows, 2) all bursty flows, and 3) a mixture of both.

1) *Streaming traffic*: When the traffic is configured with all streaming flows, the average end-to-end delays (unit: time slots) as a function of the network size for ten tested BP schemes are presented in Fig. 5(a). Although not presented in Figs. 5, the ranking of the BP schemes on packet delivery rate is consistent with the inverted ranking on latency, showing that the latency under streaming traffic is dominated by the contribution of undelivered packets, whose delays are counted as T . This is consistent with the results under mixed traffic shown in Table II (Section VII-B3).

While all the BP variations improve the latency over the basic BP, the unbiased BP-SJB and BP-HOL bring limited improvements since they still suffer from the drawbacks of slow startup and random walk. Their advantages diminish in larger networks, where those drawbacks are more pronounced. The biased SP-BP schemes substantially improve the latency, showing that the pre-defined, optimally scaled distance gradi-

ents can warm start the system and effectively mitigate random walks. Queue length-based EDR- \bar{r} achieves a latency lower than 300 time slots, whereas by incorporating additional link features, SP- $\bar{r}/(xr)$ further reduces the latency of EDR- \bar{r} by nearly a half. Applying optimal bias-scaling to SP- $\bar{r}/(xr)$ (SP- $\bar{r}/(xr)$ -min) also slightly improves its latency.

Incorporating delay-based backlog metrics, SJB and HOL, into EDR- \bar{r} can significantly degrade its performance. In contrast, $expQ$ slightly improves EDR- \bar{r} for smaller networks ($|\mathcal{V}| \leq 90$), and slightly degrades SP- $\bar{r}/(xr)$, showing that $expQ$ does less harm when applied to streaming traffic, which is not the original purpose of $expQ$.

2) *Bursty traffic*: When the traffic is configured with all bursty flows, the average end-to-end delays (unit: time slots) as a function of the network size for ten tested BP schemes under lighter and heavier traffic loads are respectively presented in Figs. 5(b) and 5(c), and the packet delivery rates corresponding to Fig. 5(c) are illustrated in Fig. 5(d). The flow rates for the lighter and heavier bursty traffic are respectively $\lambda(f) \sim \mathbb{U}(2.0, 10.0)$ and $\lambda(f) \sim \mathbb{U}(6.6, 33.0)$ for $t < 30$, and

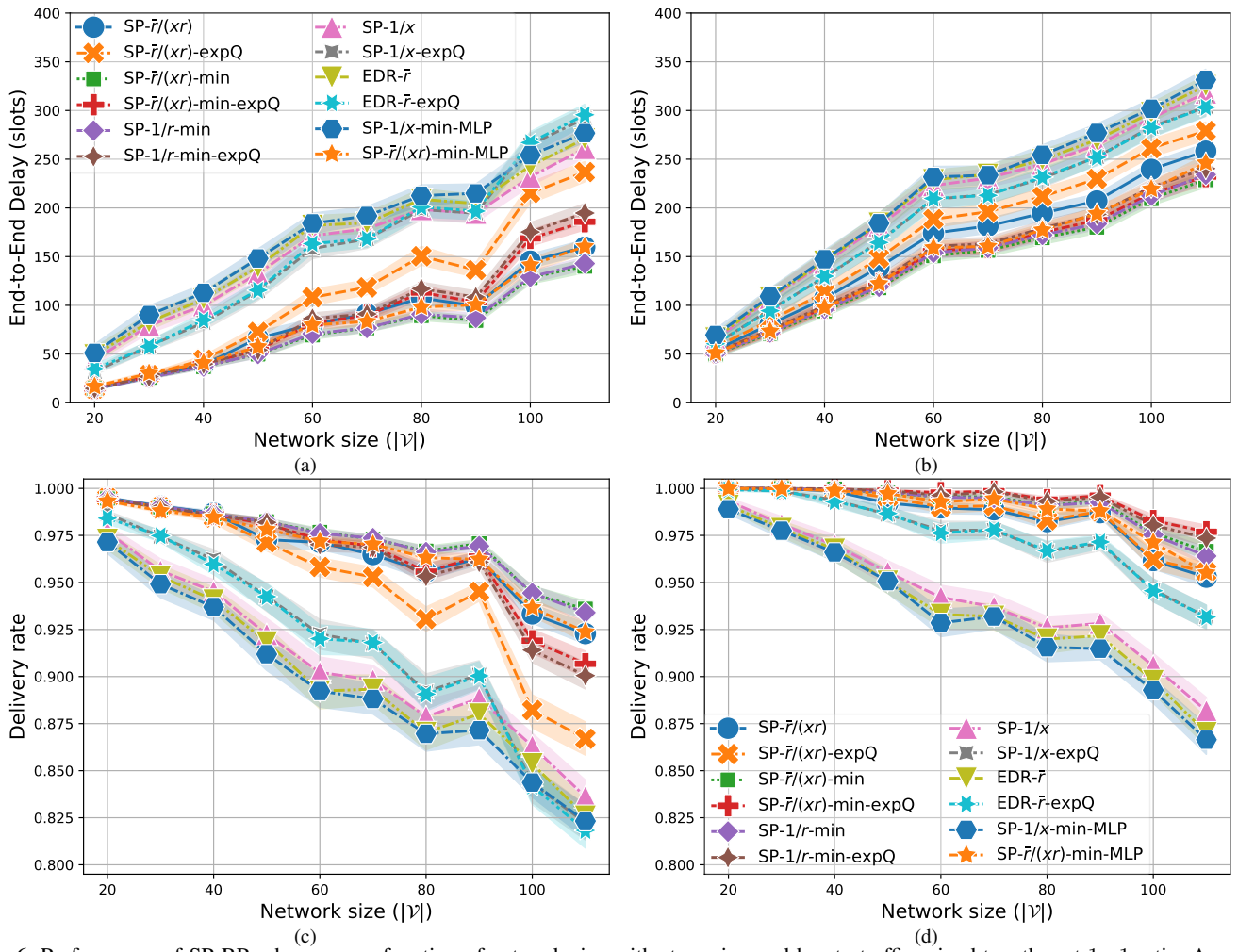


Fig. 6: Performance of SP-BP schemes as a function of network size with streaming and bursty traffic mixed together at 1 : 1 ratio. Average end-to-end delays of (a) streaming flows and (b) bursty flows. Average packet delivery rates of (c) streaming flows and (d) bursty flows. Simulated with long-term link rates $r_e \sim \mathbb{U}(10, 42)$, unit-disc interference model, total time steps $T = 1000$, and 100 test instances per point (10 random networks \times 10 realizations of random flows and link rates). Error band indicates 95% confidence interval.

$\lambda(f) = 0$ for $t \geq 30$. Compared to the cases of streaming traffic, the basic BP performs slightly better under heavier bursty traffic but worse under lighter bursty traffic, whereas both SJB and HOL can consistently improve the latency of basic BP regardless of the traffic loads.

Under bursty traffic the shortest path bias is still the most important factor for improved latency and delivery rate, evidenced by the lowest latency achieved by queue length-based $\text{SP-}\bar{r}/(\text{xr})$ and $\text{SP-}\bar{r}/(\text{xr})\text{-min}$ under both lighter and heavier traffic loads. The fact that they consistently outperform $\text{EDR-}\bar{r}$ also demonstrates that link features can better inform shortest path biases than do hop counts. Optimal bias scaling also benefits bursty traffic, as demonstrated by $\text{SP-}\bar{r}/(\text{xr})\text{-min}$ outperforming $\text{SP-}\bar{r}/(\text{xr})$ under heavier traffic loads.

Under lighter bursty traffic, both HOL and expQ can significantly improve the latency of $\text{EDR-}\bar{r}$ (Fig. 5(b)), boosting its delivery rate from 91.0% to 99.8% and 99.5%, respectively [2]. However, as the flow rates triple, they degrade the latency of $\text{EDR-}\bar{r}$ (Fig. 5(c)) but still improve its delivery rate (Fig. 5(d)). Such an increase in congestion is caused by the fact that HOL and expQ can reduce the network capacity of

biased BP, as discussed in Section VII-C. A similar effect can be observed when expQ is applied to $\text{SP-}\bar{r}/(\text{xr})$. Under lighter bursty traffic (Fig. 5(b)), $\text{SP-}\bar{r}/(\text{xr})\text{-min}$, $\text{SP-}\bar{r}/(\text{xr})$, and $\text{SP-}\bar{r}/(\text{xr})\text{-expQ}$ achieve the 1st, 2nd, and 3rd best latency, at a 100% delivery rate. However, under heavier bursty traffic, as shown in Figs. 5(c) and 5(d), expQ worsens the latency and delivery rate of $\text{SP-}\bar{r}/(\text{xr})$, while optimal bias scaling improves both performances. For biased BP, expQ consistently outperforms HOL and SJB, however, the effectiveness of these delay-based backlog metrics is limited to lighter traffic.

3) *Mixed Traffic*: We next evaluate low-overhead BP schemes under a mixture of streaming and bursty flows, to assess their effectiveness on the last packet problem under the interference of streaming traffic. In this case, a source-destination pair is configured as either streaming or bursty flow at equal probabilities. The bursty flows are configured with the heavier traffic loads described in Section VII-B2, to ensure similar numbers of packets are injected into the network for both streaming and bursty flows. We present the average latency and packet delivery rates of streaming and bursty flows under 15 tested BP schemes, alongside their

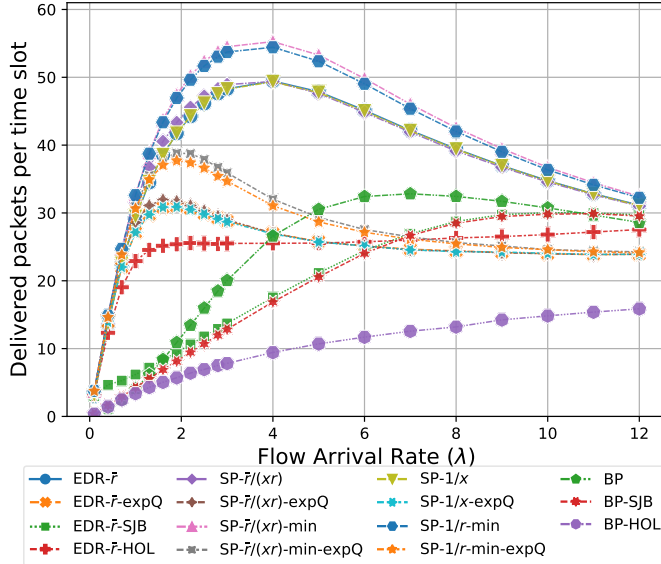


Fig. 7: Average end-to-end network throughput (number of packets delivered to their destinations per time slot across the network) under various SP-BP schemes as a function of flow arrival rate. Simulated in random networks of 100 nodes under unit-disk interference model, long-term link rates $r_e \sim \mathbb{U}(10, 42)$, total time steps $T = 1000$, and 100 test instances per point (10 random networks \times 10 realizations of random source-destination pairs and link rates).

rankings in Table II. In general, their rankings are consistent with the results in Sections VII-B1 and VII-B2 with similar traffic loads, with the exception that $expQ$ is able to improve $EDR-\bar{r}$ and $SP-\bar{r}/(xr)$ for bursty flows in mixed traffic.

We compare the performances of ten SP-BP schemes under mixed traffic, presenting their latency as a function of network size in Figs. 6(a) and 6(b) for streaming and bursty flows, respectively, and the corresponding packet delivery rates in Figs. 6(c) and 6(d). Generally, better performance can be achieved by incorporating more local and global information into the shortest path biases. Notably, $SP-1/x$ can consistently outperform $EDR-\bar{r}$ without access to any global information, whereas the latter requires the global average link rate \bar{r} . When the local long-term link rates r and the global \bar{r} become available, $SP-\bar{r}/(xr)$ can achieve performance comparable to $SP-1/r\text{-min}$, which requires additional knowledge of the global r_{\max} . With access to global $(xr)_{\max}$, $SP-\bar{r}/(xr)\text{-min}$ can achieve the best latency. These demonstrate the effectiveness of our proposed method of using GNNs to predict the link duty cycle in biased BP. The $expQ$ consistently improves the delivery rates of biased BP schemes for bursty flows, with the top two delivery rates achieved by $SP-\bar{r}/(xr)\text{-min-expQ}$ and $SP-1/r\text{-min-expQ}$ (Fig. 6(d)), demonstrating its effectiveness in solving the last packet problem.

To demonstrate the benefit of adopting GNNs in our enhanced SP-BP schemes, we replace the GCNN with a multi-layer perceptron (MLP) with the same hyperparameters (L, g_l, σ_l) and training procedure, using node degree as input feature. It can be observed from Figs. 6 that the MLP-based schemes, $SP-1/x\text{-min-MLP}$ and $SP-\bar{r}/(xr)\text{-min-MLP}$, always underperform their GCNN-based counterparts due to the inferior ability of MLP in encoding topological information.

The above results are consistent with similar tests under different node densities and interference levels without retraining the GCNN, as included in our code repository. It shows that the proposed enhancements generalize well to various scenarios.

C. Network Capacity Region

To illustrate the impact of different low-overhead BP schemes on network capacity, we test them on 10 random networks of size $|\mathcal{V}| = 100$ under streaming flows with constant arrival rates ranging from $0.1 \leq \lambda \leq 12$. The total number of packets delivered to their destinations is collected for each test instance after $T = 1000$ time steps, and the average end-to-end total throughput of 15 BP schemes as a function of flow arrival rate are presented in Fig. 7 and the corresponding peak values are listed in Table II (last column). For most BP schemes, the end-to-end total throughput first increases with the flow arrival rate, and then decreases slowly after reaching a peak. When the flow arrival rate is too large, the MaxWeight scheduler will prioritize the links near source nodes, so that fewer packets will reach their destinations, causing a decrease in the end-to-end throughput.

Since the network-wide rate of packet injection $\lambda|\mathcal{F}|$ is linear to the flow rate, the total number of backlogged packets within the network will increase rapidly after the end-to-end throughput reaches its peak. Therefore, we consider the peak end-to-end throughput as the network capacity under certain BP schemes. The basic BP reaches the network capacity of 32.83 at $\lambda = 7.0$. With optimally scaled shortest path biases derived from different levels of information access, queue length-based biased BP schemes increase the network capacity of basic BP by 50% to 68% at the same peak of $\lambda = 4.0$, while keeping their throughput always above that of basic BP. Notably, $EDR-\bar{r}$, $SP-1/x$, and $SP-\bar{r}/(xr)$ achieve almost identical maximum throughput, where $SP-\bar{r}/(xr)$ has larger throughput when $\lambda < 4.0$. The fully optimized $SP-\bar{r}/(xr)\text{-min}$ and $SP-1/r\text{-min}$ respectively achieve the best and second network capacities.

The delay-based backlog metrics, including SJB, HOL, and $expQ$, all reduce their network capacity region at different levels, paying a cost for improving delivery rates at light-weight traffic loads. Our $expQ$ keeps achieving higher network capacity than SJB and HOL, when applied to $EDR-\bar{r}$.

D. Node mobility

Lastly, we run 100 test instances on 10 draws of random networks with 100 nodes and node mobility, in which for every 100 time steps, 10 random nodes take a random step on the 2D plane, i.e., $\kappa \in \mathbb{R}^2, \kappa_i \sim \mathcal{N}(0, 0.1)$ (normal distribution with mean of zero and standard deviation of 0.01), conditioned on keeping the network connected. The long-term link rate of a

TABLE III: End-to-end delay on random networks of 100 nodes, $T = 1000$ under the unit-disk interference model and node mobility.

Bias update	EDR-̄r		SP-̄r/(xr)	
	Delay (std.)	Delivery (std.)	Delay (std.)	Delivery (std.)
Ideal	278.3 (106.1)	81.2% (8.7%)	155.2 (80.9)	90.8% (6.1%)
Neighbor	331.8 (103.8)	75.7% (9.1%)	282.5 (87.5)	78.5% (7.8%)

newly created link e is set as $r_e \sim \mathbb{U}(10, 42)$. We compare the end-to-end delay and delivery rate of our neighborhood bias update rule in (10) with those of ideal (instantaneous) SSSP in Table III. Under the practical neighborhood update rule, $\text{SP-}\bar{r}/(xr)$ suffers a larger loss from the ideal (but impractical) SSSP than $\text{EDR-}\bar{r}$, i.e., the delivery rate of $\text{SP-}\bar{r}/(xr)$ dropped by 12% compared to a drop of 5.6% with $\text{EDR-}\bar{r}$. Despite larger delays and lower delivery rates, $\text{EDR-}\bar{r}$ suffers less under node mobility, showing that it is more robust to transient errors in biases.

VIII. CONCLUSIONS

In this paper, we studied BP routing and scheduling with queue-agnostic shortest path bias, which effectively addresses the drawbacks of BP while retaining its queue stabilizing capability. Our four enhancements to SP-BP: delay-aware link weight, optimal bias scaling, low-overhead bias maintenance, and $\exp Q$ (a delay-aware backlog metric that works well with SP biases) are demonstrated to be effective in improving the latency and effective throughput of BP schemes. The benefits of our enhanced SP-BP schemes are limited to well-connected wireless networks with relatively low mobility. Further investigations are required to enable BP schemes in wireless networks that are intermittently connected or subject to varying levels of node mobility. Other potential extensions to this work include considering the uncertainties and/or shifts in link features and their global minimal/maximal values; facilitating the prediction of the link duty cycles by incorporating additional link and traffic features, such as betweenness centralities and flow arrival rates; exploring other GNN architectures such as Graph Attention Networks, and developing training techniques for faster convergence and/or continuous online learning using real-time network data.

APPENDIX A PROOF OF INEQUALITY

To prove $(\max[q - o, b] + p)^2 \leq q^2 + o^2 + p^2 + b^2 + 2bp + 2q(p - o)$ for $q \geq 0, o \geq 0, b \geq 0, p \geq 0$, consider two cases:

Case 1: $q - o \geq b$, we have

$$\begin{aligned} (\max[q - o, b] + p)^2 &= (q - o + p)^2 \\ &= q^2 + o^2 + p^2 + 2qp - 2qo - 2op \\ &\leq q^2 + o^2 + p^2 + 2q(p - o) \\ &\leq q^2 + o^2 + p^2 + b^2 + 2bp + 2q(p - o), \end{aligned}$$

since $2op \geq 0, b^2 + 2bp \geq 0$.

Case 2: $q - o < b$, we have

$$\begin{aligned} (\max[q - o, b] + p)^2 &= (b + p)^2 \\ &= b^2 + p^2 + 2bp \\ &\leq (q - o)^2 + 2qp + b^2 + p^2 + 2bp \\ &= q^2 + o^2 + p^2 + b^2 + 2bp + 2q(p - o), \end{aligned}$$

since $(q - o)^2 + 2qp \geq 0$.

With Case 1 and Case 2, we prove the inequality.

APPENDIX B

JUSTIFICATION OF LIGHTWEIGHT TRAFFIC SETTING

For all streaming flow setting, given the test setting in Section VII, in each test instance, the expected number of source nodes is $0.4|\mathcal{V}|$, each with an average arrival rate of $0.6 = (0.2 + 1.0)/2$, the average exogenous packet arrival rate per node is computed as $0.24 = 0.6 \times 0.4$.

The expected link rate of a bidirectional link is $26 = (10 + 42)/2$. With a node density of $8/\pi$, the expected number of immediate neighbors of each node is 8. Given the average conflict degree of each link as 34.6, the average maximum outflow rate per node is computed as $3 \approx (26 \times 8 \times 0.5)/34.6$, assuming an even split of link rate for both directions.

REFERENCES

- [1] Z. Zhao, B. Radojicic, G. Verma, A. Swami, and S. Segarra, “Delay-aware backpressure routing using graph neural networks,” in *IEEE Int. Conf. on Acoustics, Speech and Signal Process. (ICASSP)*, pp. 4720–4724, 2023.
- [2] Z. Zhao, G. Verma, A. Swami, and S. Segarra, “Enhanced backpressure routing using wireless link features,” in *IEEE Intl. Wrksp. Comput. Advances Multi-Sensor Adaptive Process. (CAMSAP)*, pp. 1–5, Dec. 2023.
- [3] L. Tassiulas and A. Ephremides, “Stability properties of constrained queueing systems and scheduling policies for maximum throughput in multihop radio networks,” *IEEE Trans. on Automatic Control*, vol. 37, no. 12, pp. 1936–1948, 1992.
- [4] X. Lin, N. B. Shroff, and R. Srikant, “A tutorial on cross-layer optimization in wireless networks,” *IEEE J. Sel. Areas Commun.*, vol. 24, no. 8, pp. 1452–1463, 2006.
- [5] S. K. Sarkar, T. G. Basavaraju, and C. Puttamadappa, *Ad hoc Mobile Wireless Networks: Principles, Protocols and Applications*. CRC Press, 2013.
- [6] A. Kott, A. Swami, and B. J. West, “The internet of battle things,” *Computer*, vol. 49, no. 12, pp. 70–75, 2016.
- [7] N. Patriciello, C. A. Grajia, J. Núñez-Martínez, J. Baranda, J. Mangues-Bafalluy, and M. Casoni, “Performance evaluation of backpressure routing in integrated satellite-terrestrial backhaul for PPDR networks,” in *2016 IEEE 12th International Conference on Wireless and Mobile Computing, Networking and Communications (WiMob)*, pp. 1–8, 2016.
- [8] I. F. Akyildiz, A. Kak, and S. Nie, “6G and beyond: The future of wireless communications systems,” *IEEE Access*, vol. 8, pp. 133995–134030, 2020.
- [9] “Cisco annual internet report (2018–2023),” white paper, Cisco Systems, Inc., Mar. 2020. <https://www.cisco.com/c/en/us/solutions/collateral/executive-perspectives/annual-internet-report/white-paper-c11-741490.html>, accessed June 2023.
- [10] X. Chen, D. W. K. Ng, W. Yu, E. G. Larsson, N. Al-Dhahir, and R. Schober, “Massive access for 5G and beyond,” *IEEE J. Sel. Areas Commun.*, vol. 39, no. 3, pp. 615–637, 2021.
- [11] M. Cudak, A. Ghosh, A. Ghosh, and J. Andrews, “Integrated access and backhaul: A key enabler for 5G millimeter-wave deployments,” *IEEE Communications Magazine*, vol. 59, no. 4, pp. 88–94, 2021.
- [12] M. J. Neely, E. Modiano, and C. E. Rohrs, “Dynamic power allocation and routing for time-varying wireless networks,” *IEEE J. Sel. Areas Commun.*, vol. 23, no. 1, pp. 89–103, 2005.
- [13] L. Georgiadis, M. J. Neely, and L. Tassiulas, “Resource allocation and cross-layer control in wireless networks,” *Foundations and Trends® in Networking*, vol. 1, no. 1, pp. 1–144, 2006.
- [14] M. Neely, *Stochastic network optimization with application to communication and queueing systems*. Springer Nature, 2022.
- [15] Z. Jiao, B. Zhang, W. Gong, and H. Mouftah, “A virtual queue-based back-pressure scheduling algorithm for wireless sensor networks,” *EURASIP J. on Wireless Commun. and Netw.*, vol. 2015, no. 1, pp. 1–9, 2015.
- [16] Y. Cui, E. M. Yeh, and R. Liu, “Enhancing the delay performance of dynamic backpressure algorithms,” *IEEE/ACM Trans. Netw.*, vol. 24, no. 2, pp. 954–967, 2016.
- [17] J. Gao, Y. Shen, M. Ito, and N. Shiratori, “Bias based general framework for delay reduction in backpressure routing algorithm,” in *Intl. Conf. Computing, Networking and Communications (ICNC)*, pp. 215–219, IEEE, 2018.

- [18] M. Alresaini, K.-L. Wright, B. Krishnamachari, and M. J. Neely, "Back-pressure delay enhancement for encounter-based mobile networks while sustaining throughput optimality," *IEEE/ACM Trans. Netw.*, vol. 24, no. 2, pp. 1196–1208, 2016.
- [19] B. Ji, C. Joo, and N. B. Shroff, "Delay-based back-pressure scheduling in multihop wireless networks," *IEEE/ACM Trans. Netw.*, vol. 21, no. 5, pp. 1539–1552, 2012.
- [20] E. Athanasopoulou, L. X. Bui, T. Ji, R. Srikanth, and A. Stolyar, "Back-pressure-based packet-by-packet adaptive routing in communication networks," *IEEE/ACM Trans. Netw.*, vol. 21, no. 1, pp. 244–257, 2012.
- [21] L. Hai, Q. Gao, J. Wang, H. Zhuang, and P. Wang, "Delay-optimal back-pressure routing algorithm for multihop wireless networks," *IEEE Trans. Vehicular Tech.*, vol. 67, no. 3, pp. 2617–2630, 2018.
- [22] A. Rai, C.-p. Li, G. Paschos, and E. Modiano, "Loop-free backpressure routing using link-reversal algorithms," *IEEE/ACM Trans. Netw.*, vol. 25, no. 5, pp. 2988–3002, 2017.
- [23] P. Yin, S. Yang, J. Xu, J. Dai, and B. Lin, "Improving backpressure-based adaptive routing via incremental expansion of routing choices," in *ACM/IEEE Symp. Arch. for Networking and Communications Systems (ANCS)*, pp. 1–12, IEEE, 2017.
- [24] L. Ying, S. Shakkottai, A. Reddy, and S. Liu, "On combining shortest-path and back-pressure routing over multihop wireless networks," *IEEE/ACM Trans. Netw.*, vol. 19, no. 3, pp. 841–854, 2010.
- [25] L. Ying and S. Shakkottai, "Scheduling in mobile ad hoc networks with topology and channel-state uncertainty," *IEEE Trans. on Automatic Control*, vol. 57, no. 10, pp. 2504–2517, 2012.
- [26] J. Ryu, L. Ying, and S. Shakkottai, "Timescale decoupled routing and rate control in intermittently connected networks," *IEEE/ACM Trans. Netw.*, vol. 20, no. 4, pp. 1138–1151, 2012.
- [27] C. Liaskos, K. Alexandris, A. Das, S. Tang, and L. Tassiulas, "Analysis and evaluation of fully TCP-compatible backpressure-driven traffic engineering," *IEEE Transactions on Network Science and Engineering*, vol. 10, no. 6, pp. 4056–4070, 2023.
- [28] C. Joo and N. B. Shroff, "Local greedy approximation for scheduling in multihop wireless networks," *IEEE Trans. on Mobile Computing*, vol. 11, no. 3, pp. 414–426, 2012.
- [29] Z. Zhao, G. Verma, C. Rao, A. Swami, and S. Segarra, "Distributed scheduling using graph neural networks," in *IEEE Int. Conf. on Acoustics, Speech and Signal Process. (ICASSP)*, pp. 4720–4724, 2021.
- [30] D. Katsaros, N. Dimokas, and L. Tassiulas, "Social network analysis concepts in the design of wireless ad hoc network protocols," *IEEE Network*, vol. 24, no. 6, pp. 23–29, 2010.
- [31] Z. Wu, S. Pan, F. Chen, G. Long, C. Zhang, and S. Y. Philip, "A comprehensive survey on graph neural networks," *IEEE Trans. on Neural Networks and Learning Systems*, 2020.
- [32] A. Sinha and E. Modiano, "Optimal control for generalized network-flow problems," *IEEE/ACM Transactions on Networking*, vol. 26, no. 1, pp. 506–519, 2018.
- [33] Q. M. Nguyen, M. S. Rahman, X. Fu, S. Kompella, J. Macker, and E. H. Modiano, "An optimal network control framework for wireless SDN: From theory to implementation," in *IEEE Military Comms. Conf. (MILCOM)*, pp. 102–109, 2022.
- [34] A. Chowdhury, G. Verma, C. Rao, A. Swami, and S. Segarra, "ML-aided power allocation for tactical MIMO," in *IEEE Military Comms. Conf. (MILCOM)*, pp. 273–278, IEEE, 2021.
- [35] A. Chowdhury, G. Verma, C. Rao, A. Swami, and S. Segarra, "Unfolding WMMSE using graph neural networks for efficient power allocation," *IEEE Trans. Wireless Commun.*, vol. 20, no. 9, pp. 6004–6017, 2021.
- [36] A. Chowdhury, G. Verma, A. Swami, and S. Segarra, "Deep graph unfolding for beamforming in MU-MIMO interference networks," *IEEE Trans. Wireless Commun.*, 2023. (Early Access).
- [37] B. Li, G. Verma, and S. Segarra, "Graph-based algorithm unfolding for energy-aware power allocation in wireless networks," *IEEE Trans. Wireless Commun.*, 2022.
- [38] M. Eisen and A. Ribeiro, "Optimal wireless resource allocation with random edge graph neural networks," *IEEE Trans. Signal Process.*, 2020.
- [39] Z. Wang, L. Ruiz, M. Eisen, and A. Ribeiro, "Stable and transferable wireless resource allocation policies via manifold neural networks," in *IEEE Int. Conf. on Acoustics, Speech and Signal Process. (ICASSP)*, pp. 8912–8916, 2022.
- [40] Y. Shen, J. Zhang, S. H. Song, and K. B. Letaief, "Graph neural networks for wireless communications: From theory to practice," *IEEE Trans. Wireless Commun.*, vol. 22, no. 5, pp. 3554–3569, 2023.
- [41] B. Li, J. Perazzone, A. Swami, and S. Segarra, "Learning to transmit with provable guarantees in wireless federated learning," *IEEE Trans. Wireless Commun.*, 2023. accepted for publication.
- [42] Z. Zhao, G. Verma, A. Swami, and S. Segarra, "Delay-oriented distributed scheduling using graph neural networks," in *IEEE Int. Conf. on Acoustics, Speech and Signal Process. (ICASSP)*, pp. 8902–8906, 2022.
- [43] Z. Zhao, A. Swami, and S. Segarra, "Distributed link sparsification for scalable scheduling using graph neural networks," in *IEEE Int. Conf. on Acoustics, Speech and Signal Process. (ICASSP)*, pp. 5308–5312, 2022.
- [44] Z. Zhao, G. Verma, C. Rao, A. Swami, and S. Segarra, "Link scheduling using graph neural networks," *IEEE Trans. Wireless Commun.*, vol. 22, no. 6, pp. 3997–4012, 2023.
- [45] M. Lee, G. Yu, and G. Y. Li, "Graph embedding-based wireless link scheduling with few training samples," *IEEE Trans. Wireless Commun.*, vol. 20, no. 4, pp. 2282–2294, 2021.
- [46] Z. Zhao, A. Swami, and S. Segarra, "Graph-based deterministic policy gradient for repetitive combinatorial optimization problems," in *The Eleventh International Conference on Learning Representations*, 2023.
- [47] X. Li, Y. Xiao, S. Liu, X. Lu, F. Liu, W. Zhou, and J. Liu, "GAPPO - a graph attention reinforcement learning based robust routing algorithm," in *IEEE 34th Annual International Symposium on Personal, Indoor and Mobile Radio Communications (PIMRC)*, pp. 1–7, 2023.
- [48] K. Rusek, J. Suárez-Varela, P. Almasan, P. Barlet-Ros, and A. Cabellos-Aparicio, "RouteNet: Leveraging graph neural networks for network modeling and optimization in SDN," *IEEE Journal on Selected Areas in Communications*, vol. 38, no. 10, pp. 2260–2270, 2020.
- [49] B. Li, T. Efimov, A. Kumar, J. Cortes, G. Verma, A. Swami, and S. Segarra, "Learnable digital twin for efficient wireless network evaluation," in *IEEE Military Comms. Conf. (MILCOM)*, pp. 661–666, 2023.
- [50] J. Zhang, P. Yu, L. Feng, W. Li, M. Zhao, X. Yan, and J. Wu, "Fine-grained service offloading in B5G/6G collaborative edge computing based on graph neural networks," in *ICC 2022 - IEEE International Conference on Communications*, pp. 5226–5231, 2022.
- [51] Z. Zhao, J. Perazzone, G. Verma, and S. Segarra, "Congestion-aware distributed task offloading in wireless multi-hop networks using graph neural networks," 2023. Accepted to IEEE ICASSP 2024.
- [52] W. Cheng, X. Cheng, T. Znati, X. Lu, and Z. Lu, "The complexity of channel scheduling in multi-radio multi-channel wireless networks," in *IEEE Intl. Conf. on Computer Comms. (INFOCOM)*, pp. 1512–1520, 2009.
- [53] C. Joo, G. Sharma, N. B. Shroff, and R. R. Mazumdar, "On the complexity of scheduling in wireless networks," *EURASIP J. on Wireless Commun. and Netw.*, vol. 2010, no. 1, p. 418934, 2010.
- [54] R. Bellman, "On a routing problem," *Quarterly of Applied Mathematics*, vol. 16, no. 1, pp. 87–90, 1958.
- [55] L. R. Ford Jr, "Network flow theory," tech. rep., Rand Corp Santa Monica CA, 1956.
- [56] A. Bernstein and D. Nanongkai, "Distributed exact weighted all-pairs shortest paths in near-linear time," in *ACM SIGACT Symp. Theory of Comp.*, pp. 334–342, 2019.
- [57] E. W. Dijkstra, "A note on two problems in connexion with graphs," *Numerische mathematik*, vol. 1, no. 1, pp. 269–271, 1959.